2009

Control of Viscous Fingering Patterns in a Radial Hele-Shaw Cell

Shuwang Li

John S. Lowengrub

Jake Fontana

Peter Palffy-Muhoray
Kent State University - Kent Campus, mpalffy@cpip.kent.edu

Control of Viscous Fingering Patterns in a Radial Hele-Shaw Cell

Shuwang Li*
Department of Applied Mathematics, Illinois Institute of Technology, Chicago, Illinois 60616, USA

John S. Lowengrub†
Department of Mathematics, University of California, Irvine, California 92697, USA

Jake Fontana‡
Liquid Crystal Institute, Kent State University, Kent, Ohio 44242, USA

Peter Palffy-Muhoray§
Liquid Crystal Institute, Kent State University, Kent, Ohio 44242, USA
(Received 25 November 2008; published 30 April 2009)

We study numerically and experimentally the dynamics and control of viscous fingering patterns in a circular Hele-Shaw cell. The nonlocality and nonlinearity of the system, especially interactions among developing fingers, make the emergent pattern difficult to predict and control. By controlling the injection rate of the less viscous fluid, we can precisely suppress the evolving interfacial instabilities. There exist denumerable attractive, self-similarly evolving symmetric, universal shapes. Experiments confirm the feasibility of the control strategy, which is summarized in a morphology diagram.

DOI: 10.1103/PhysRevLett.102.174501 PACS numbers: 47.15.gp, 47.20.Hw, 47.54.−r, 47.55.N−

A variety of pattern forming phenomena, ranging from the growth of bacterial colonies to snowflake formation, share similar underlying physical mechanisms and mathematical structure. Viscous fingering, considered here, is a paradigm for such phenomena. Dense-branching or dendritic morphologies are among the most common forms of microstructural patterning in systems driven out of equilibrium [1–3]. The interest in understanding the formation kinetics and the interplay of system parameters is to provide understanding of growth and form in nature as well as to achieve improved control and efficiency in a variety of physical, biological, and engineering systems. Prediction and control of the shape of emergent patterns are both difficult due to the nonlocality and nonlinearity of the system.

In a Hele-Shaw cell [4], Saffman and Taylor [5] demonstrated, using linear stability theory, that when air is injected into a viscous fluid at a constant pressure or injection rate, the interface becomes unstable and develops a fingered pattern. Though surface tension suppresses the growth of perturbations, linear theory predicts that successively higher wave number perturbations become unstable as the air bubble grows (see Fig. 1). Nonlinear interactions among different modes then become important and the nonlinear evolution leads to the usual dense-branching morphologies [5–13].

In a theoretical study of viscous fingers in 90° sector geometry, Brener *et al.* [14] suggested that if the injection rate instead scales with time like $t^{-1/3}$ it may be possible to obtain self-similar growing single fingers for finite surface tension, thus avoiding the dense-branching morphology regime. Indeed, this is the unique scaling for which nonlinear self-similar evolution can be obtained [14–16]. Sector geometries, introduced in experiments by Thome *et al.* [17], are a generalization of the channel geometry with parallel walls [5]. Growth of fingers in the sector

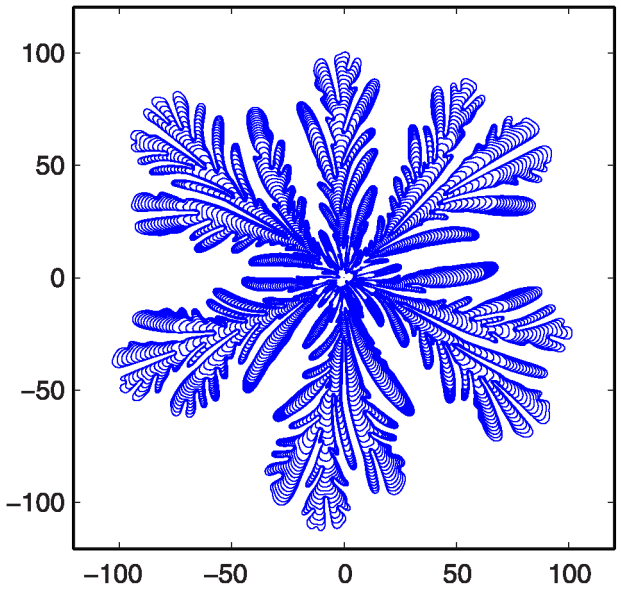

FIG. 1 (color online). Numerical simulation of a highly ramified bubble in the nonlinear regime expanding under a constant flux. A time sequence of bubble shapes is shown that tend towards a dense-branching morphology. This is the largest and most pronounced viscous fingering simulation to date and uses the algorithm developed by Li *et al.* [13].

geometry mimics the growth in a circular geometry in the special case that the fingers do not interact. In a range of sector geometries, Tu [18] obtained analytic solutions for zero-surface tension fingers and used the WKB perturbation method to investigate the effect of small surface tension and finger selection. Combescot and Ben Amar [15] and Ben Amar *et al.* [19] found numerically self-similar divergent (and convergent) fingers with finite surface tension.

In this Letter, we consider the full circular geometry under the $t^{-1/3}$ scaling of the injection rate and investigate the pattern forming dynamics during long-time evolution. We observe that there are significant finger-finger interactions at the early stages where new fingers are created by tip-splitting and fingers disappear. Starting from an arbitrary shape, the long-time evolution leads to compact shapes that depend only on the prefactor (see below) of the injection rate. These attractive shapes grow self-similarly. The attractive shapes are stable in the sense that shape perturbations decay. Although these shapes are symmetric and thus could be described by a single finger (as in the sector geometry), we show that the solutions are different from those reported in [15,19]. We construct a morphology diagram that illustrates the relation between the symmetry of the attractive shapes and the prefactor. In proof-of-concept experiments, we have varied the air injection rate according to the morphology diagram to control the shape of viscous fingering patterns, thereby confirming the feasibility of this strategy.

Given a circular air-oil interface slightly perturbed by an azimuthal Fourier mode with wave number k, the interface will evolve in the linear regime as $r(t,\theta) = R(t) + \delta_k(t) \times \cos k\theta$, where $r(t,\theta)$ and $R(t)$ are the radius of the perturbed and unperturbed air-fluid interface, respectively, and $\delta_k(t)$ is the amplitude of the perturbation. The radius $R(t)$ satisfies $\frac{d}{dt}(b\pi R^2) = J(t)$ where b is the gap between the two plates in the Hele-Shaw cell and $J(t)$ is the volume flux of the injected air. A classical linear stability analysis [20,21] yields the growth rate of the perturbation as $(\frac{\delta_k}{R})^{-1}\frac{d}{dt}(\frac{\delta_k}{R}) = \frac{k-2}{R^2}(J(t) - J_k(t))$ where the critical flux $J_k(t) = \frac{k(k^2-1)}{k-2}J_\sigma(R)$ and $J_\sigma(R) = \frac{b^2}{12\mu}\frac{\sigma}{R^2}2\pi bR$ is the intrinsic characteristic flux of a bubble of radius R due to the surface tension σ (μ is the viscosity of the fluid). Thus, a perturbation with wave number k grows (decays) if the applied flux $J = J(t)$ is larger (smaller) than $J_k(t)$. When $J(t) = J_k(t)$, the growth rate of the perturbation is zero. When $J(t) = J_k^*(t)$, where $J_k^*(t) = (3k^2 - 1)J_\sigma(R)$, the kth mode has the largest growth rate among all the modes. Taking $J(t) = CJ_\sigma(R)$ [14,15,19], where the prefactor C is a dimensionless constant, the radius grows like $R(t) \sim t^{1/3}$ and according to linear theory, both the number of unstable modes and the fastest growth mode do not change as the interface expands. Note that C is the only dimensionless parameter needed to characterize the system.

In Fig. 2, the nonlinear evolution of the overall shape perturbation (the maximum deviation of the interface from the equivalent circle) is shown as a function of the equivalent radius for three different initial conditions with flux as above with $C = 84$. Insets show time sequences of the corresponding shapes. The nonlinear equations are solved in a radial domain that extends to infinity using a new, highly efficient method developed by Li *et al.* [13] that improves upon earlier work of Hou *et al.* [22]. The algorithm utilizes a novel time-space rescaling scheme to perform spectrally accurate very long-time simulations.

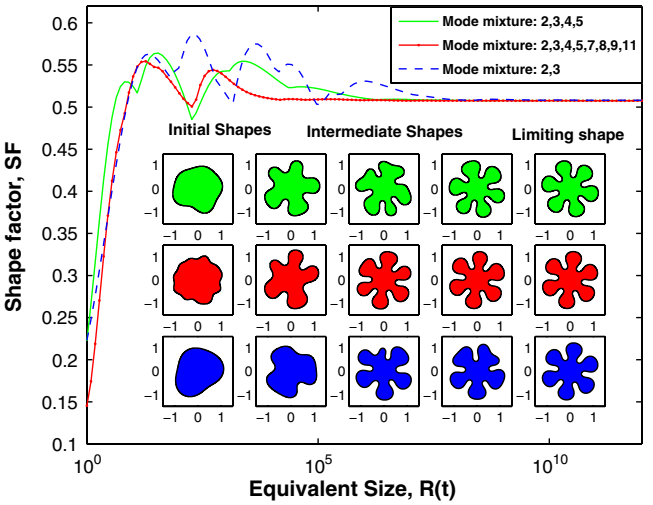

FIG. 2 (color online). The nonlinear evolution of the overall shape perturbation [maximum deviation from a circle with the same area (equivalent circle)] for three different initial conditions with flux $J(t) = C\frac{\sigma b^2}{12\mu}\frac{2\pi b}{R(t)}$, where $C = 84$ and $R(t)$ is the radius of the equivalent circle. Note that $R(t)$ is independent of bubble shape. The initial conditions contain the modes listed in the figure. The self-similar shape that is obtained at long times depends only on the dimensionless parameter C.

Linear theory predicts that mode 6 is the fastest growth mode for the flux $C = 84$. At early times, unstable growth is significant, and there are complicated tip-splitting and merging events. At later times, a nonlinear stabilization emerges and the system evolves towards a sixfold attracting, self-similar shape. Though the three limiting shapes differ by a rotation, the shape itself is the same. The attracting, limiting shape has a striking sixfold symmetric pattern with circles tangent to the inner troughs and the outer fingertips. The nonlinear limiting shape contains all harmonics of mode 6 (i.e., modes 6, 12, 18, etc.).

These results are completely outside the predictions of linear theory. Mode 6, not present in the initial data, is first created by nonlinear interactions and then is selected as the fastest growing mode. However, rather than growing exponentially, as is predicted by linear stability theory, the growth of all the modes stabilizes due to nonlinear interactions. Even though the initial data differ significantly, all three simulations converge to the same self-similarly evolving, nonlinear limiting shape that is far from circular and is clearly not a dense-branching morphology. This result strongly suggests that the limiting shape is universal

in the sense that it depends only on the flux constant C and is initial data independent and, as shown in the figure, persists for over 10 orders of magnitude. These results are in contrast to the statistical equilibria observed in the dense-branching morphology regime.

As suggested above, C holds the key to a morphological selection criterion. Exploring this idea further, we perform a set of nonlinear simulations using different fluxes and a variety of initial conditions. In each case, we found evolution towards a universal limiting shape that is dictated solely by the dimensionless flux constant C. The results are summarized in a morphology diagram [Fig. 3(a)], in analogy with a phase diagram for systems in equilibrium, where a piecewise constant (staircase) curve relates the symmetry of the limiting shapes to C. There are sharp transitions from the k fold to the $(k+1)$-fold symmetries as there is a bifurcation from one family of stable solutions to another. For flux constants less then 24, approximately, the only stable self-similar solutions are circles. The length of each step increases as the flux constant increases suggesting that a broader range of fluxes can be used to achieve higher symmetries. In Fig. 3(a), we also include the results of linear theory (dashed curve) for the wave number k of the fastest growing mode. While linear theory does provide a good estimate for the symmetry of the limiting shape (indeed the Rayleigh criterion [23] predicts that only the fastest growing mode is observed in practice) there is no theory that predicts the nonlinear stabilization and saturation reported here. The development of such a nonlinear theory is an important task for future research.

In Fig. 3(b), we present parameter λ that measures the width of a single finger of the k-fold symmetric attractive shapes relative to the sector angle. Following [19], $\lambda = \theta/\theta_0$ where $\theta_0 = 360°/k$ (dashed lines) and θ is the angle of a ray emanating from the origin that is tangent to the limiting finger (solid lines). Unlike the monotonic increasing dependence of λ on θ_0 reported in [19], we find that $\lambda \approx 0.7$ for $k \geq 5$. For example, when $k = 8$ and $\theta_0 = 22.5°$, we obtain $\lambda = 0.73$. In Fig. 4(a) from [19], it was found that when $\theta_0 = 23°$, the corresponding width is $\lambda = 0.64$ which demonstrates a quantitative difference between the sector and circular geometry results. Moreover, for $k = 3$ and 4, it is not possible to define θ in this way since there are no rays emanating from the origin that are tangent to the finger [see Fig. 3(a)]. Further, for $k \geq 6$, the fingers are retrograde unlike the sector geometry solutions.

The morphology diagram can be used to design a nonlinear protocol in a physical experiment to control the nonlinear morphological evolution. In recent proof-of-concept experiments, we have successfully controlled the air injection rate according to the morphology diagram such that a selected mode has the fastest growth rate and would give the symmetry of the universal shape. Starting with a small initial bubble of fixed radius, the injection pressure is varied to impose the specified air injection rate. See Fig. 4(a) for a comparison between the experimental and theoretical values for the equivalent radius and the

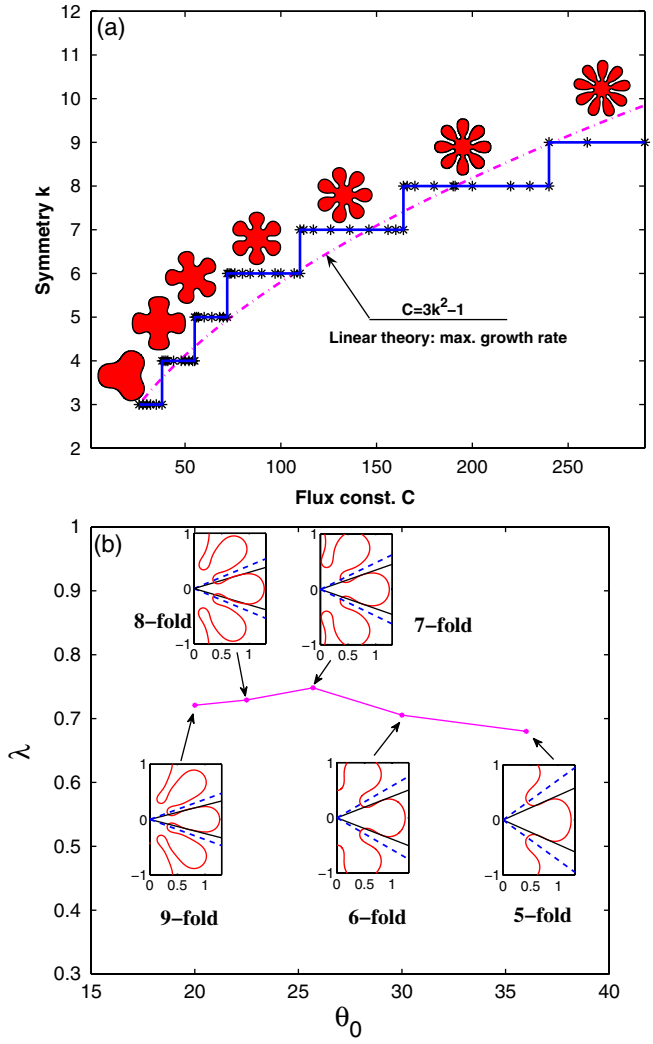

FIG. 3 (color online). The morphology diagram and characteristics of the universal shapes. (a) The morphology diagram that relates the symmetry of the universal shapes to the flux constant C. Representative universal shapes are shown. The stars denote nonlinear numerical results. The dot-dashed curve indicates the relation for the mode number k of the maximum growth rate from linear theory. There are sharp transitions from the k fold to the $(k+1)$-fold symmetries. (b) The relationship between the width λ of a single finger relative to the sector angle θ_0 of k-fold universal shapes with $k \geq 5$. Following [19], $\lambda = \theta/\theta_0$ where $\theta_0 = 360°/k$ (dashed lines) and θ is the angle of a ray emanating from the origin that is tangent to the limiting finger (solid lines).

injection pressure (such that mode 5 should be the fastest growing). Note the $t^{1/3}$ growth rate of the radius and the excellent agreement between theory and experiment. In Fig. 4(b), the corresponding evolution of the experimental bubble towards a 5-mode dominated shape is seen. At early times, there is good agreement between the numerical and experimental bubble morphologies. At later times, the boundary conditions at the outer edge of the cell become important and introduce additional effects not modeled in the simulation. Taking instead an injection flux that favors mode 8 also yields evolution towards an eightfold symme-

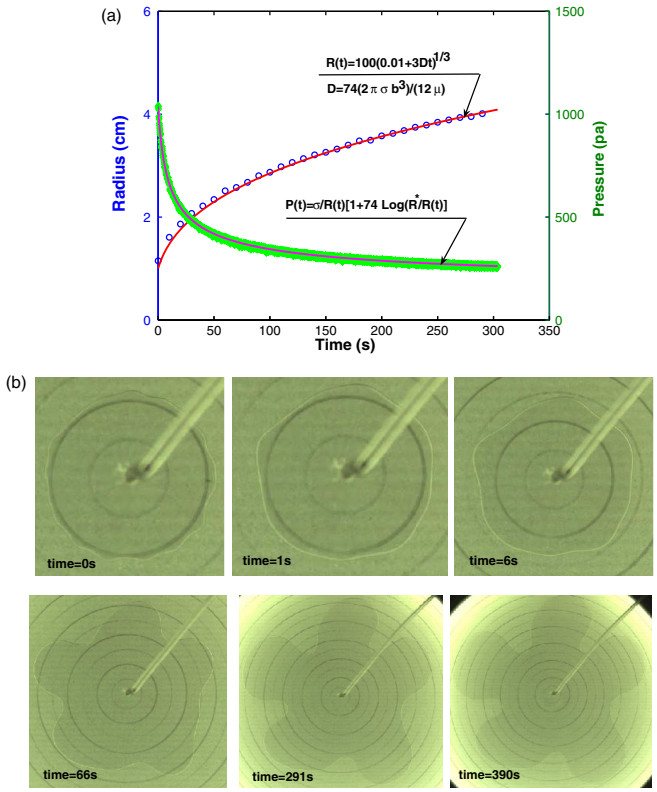

FIG. 4 (color online). Experimental demonstration that the symmetry of an expanding bubble in castor oil ($\sigma = 0.048$ N/m, $\mu = 1$ Pa · s, $b = 0.5$ mm, the size of the cell is $R^* = 10$ cm) can be selected using the flux $J(t) = C\frac{\sigma b^2}{12\mu}\frac{2\pi b}{R(t)}$. Note that there is a unique relation between the injection flux and pressure as indicated in the figure. In (a), the pressure and equivalent radius are shown-symbols (experiments), solid lines (theory)-with $C = 74$. In (b), a corresponding sequence of bubble morphologies is shown. As predicted by the morphology diagram, a fivefold shape emerges. Concentric circles mark radial increments of 0.5 cm.

try as predicted (not shown). In future work, larger cells will be used to further verify convergence to universal shapes.

In conclusion, we have suggested the existence of attractive, symmetric universal shapes in a circular Hele-Shaw cell. An open question is whether these shapes have an underlying physical interpretation. In the context of crystal growth, for instance, there is a connection between the asymptotic limit of a crystal growing with normal velocity equal to a (possibly anisotropic) mobility function and the Wulff (equilibrium) shape [24–28]. It can be shown that for any asymptotic shape there is a unique, convex surface energy density such that this shape is the minimizer of an appropriately rescaled total surface energy [26,27]. The connection of these results to the problem studied here merits further investigation.

We thank Joseph Keller, Robert Kohn, Stanley Osher, and Michael Shelley for stimulating discussions and for very helpful comments on the Letter. We acknowledge support from the NSF, Division of Mathematical Sciences. Supporting Online Material is posted on http://math.uci.edu/ lowengrb/RESEARCH/pattern.php.

*sli@math.iit.edu
†lowengrb@math.uci.edu
‡jfontana@lci.kent.edu
§mpalffy@cpip.kent.edu

[1] J. S. Langer, Science **243**, 1150 (1989).
[2] E. Ben-Jacob and P. Garik, Nature (London) **343**, 523 (1990).
[3] J. S. Langer, Rev. Mod. Phys. **52**, 1 (1980).
[4] H. S. Hele-Shaw, Nature (London) **58**, 34 (1898).
[5] P. G. Saffman and G. Taylor, Proc. R. Soc. A **245**, 312 (1958).
[6] O. Praud and H. L. Swinney, Phys. Rev. E **72**, 011406 (2005).
[7] H. Z. Cummins, L. Fourtune, and M. Rabaud, Phys. Rev. E **47**, 1727 (1993).
[8] C. W. Park, S. Gorell, and G. M. Homsy, J. Fluid Mech. **141**, 275 (1984).
[9] J. W. McLean and P. G. Saffman, J. Fluid Mech. **102**, 455 (1981).
[10] E. Ben-Jacob, G. Deutscher, P. Garik, N. D. Goldenfeld, and Y. Lareah, Phys. Rev. Lett. **57**, 1903 (1986).
[11] R. L. Chuoke, P. Van Meurs, and C. Vander Poel, Trans. Metall. Soc. AIME **216**, 188 (1959).
[12] J. V. Maher, Phys. Rev. Lett. **54**, 1498 (1985).
[13] S. W. Li, J. S. Lowengrub, and P. H. Leo, J. Comput. Phys. **225**, 554 (2007).
[14] E. A. Brener, D. Kessler, H. Levine, and W. Rappel, Europhys. Lett. **13**, 161 (1990).
[15] R. Combescot and M. Ben Amar, Phys. Rev. Lett. **67**, 453 (1991).
[16] S. W. Li, J. S. Lowengrub, P. H. Leo, and V. Cristini, J. Cryst. Growth **267**, 703 (2004).
[17] H. Thome, M. Rabaud, V. Hakim, and Y. Couder, Phys. Fluids A **1**, 224 (1989).
[18] Y. Tu, Phys. Rev. A **44**, 1203 (1991).
[19] Martine Ben Amar, V. Hakim, M. Mashaal, and Y. Couder, Phys. Fluids A **3**, 1687 (1991).
[20] L. Paterson, J. Fluid Mech. **113**, 513 (1981).
[21] A. Buka and P. Palffy-Muhoray, Phys. Rev. A **36**, 1527 (1987).
[22] T. Y. Hou, J. S. Lowengrub, and M. J. Shelley, J. Comput. Phys. **114**, 312 (1994).
[23] L. Rayleigh, Proc. London Math. Soc. **s1-10**, 4 (1878).
[24] R. Gross, Abhandl. Math.-Phys. Klasse Kongl. Sachs. Wiss **34**, 137 (1918).
[25] A. A. Chernov, Sov. Phys. Crystallogr. **7**, 728 (1963).
[26] P. Soravia, Nonlinear Analysis: Theory, Methods & Applications **22**, 1247 (1994).
[27] S. Osher and B. Merriman, Asian Math. J. **1**, 560 (1997).
[28] G. Wulff, Z. Kristallogr. Mineral. **34**, 449 (1901).